J Therm Anal Calorim (2010) 101:893–898
DOI 10.1007/s10973-010-0700-5

Initial stages of oxidation of a precipitation-hardening (PH) steel

G. Vourlias · N. Pistofidis · P. Psyllaki · E. Pavlidou · K. Chrissafis

Received: 18 August 2009 / Accepted: 21 January 2010 / Published online: 17 February 2010
© Akadémiai Kiadó, Budapest, Hungary 2010

Abstract The oxidation of a precipitation-hardening (PH) steels is a rather unexplored area. In this study an attempt is made to estimate the oxidation mechanism and the kinetics that take place up to 850 °C. For this purpose specimens of the material under examination were isothermally heated at 725, 775, 800, 825, and 850 °C for 12 h in O_2 atmosphere. The as-treated samples were examined with SEM and XRD, while kinetics were based on thermogravimetric (TG) results. From this examination it was deduced that the oxidation of this steel is accomplished at minimum three steps, following the changes of the scale morphology and the kinetics. After 850 °C although that the oxidation rate increases, the scale morphology does not change. From the calculations of the rate constant k_p and the activation energy for the phenomena below 850 °C, it was deduced that the oxidation phenomena during this stage provides another barrier to the deterioration of the ferrous material.

Keywords Steel · Oxidation · Scanning electron microscopy (SEM) · Thermogravimetry (TG)

Introduction

Although steel is a material with many advantages (such as mechanical strength and low cost), it is prone to oxidation. The principal phenomena that take place during oxidation could be divided in two main stages. The first one includes the adsorption of atomic oxygen on the metal surface, the nucleation of oxides at favorable sites and the formation of a complete thin film, while during the second stage the thickness of the initial film increases resulting to the formation of scale [1–5]. Oxidation continues with diffusion through this scale. However, the second stage could be divided in different "sub-stages," where different mechanisms are predominant and consequently different kinetic equations are applied [1–5]. The above-mentioned phenomena are well studied regarding traditional alloys. However, modern alloys, such as the precipitation-hardening (PH) steel [6–8] with the chemical composition reported in Table 1, have not been adequately studied.

The oxidation mechanism and the kinetics of the steel under question were recently investigated [7, 8], as far as it regards phenomena that take place at high temperatures and for long exposure periods. Hence, only the second stage (as previously described) was examined and actually this study was limited only to phenomena that take place at "steady-state," e.g., when the scale thickness is considerable. Possible transitional situations during the initial steps of the growth of the scale were ignored. Thus the aim of this study is to enlighten this period of the oxidation of the new PH steel. Nevertheless, the processes involving the oxygen adsorption and the oxide nucleation, along with the behavior of the initially formed thin film oxide, are not investigated separately in this study. Their effect is incorporated in the kinetic equations of the overall phenomenon.

Experimental

The material used was machined in rectangular specimens with dimensions 5 × 3 × 2 mm, while their surface was

G. Vourlias · N. Pistofidis · E. Pavlidou · K. Chrissafis (✉)
Department of Physics, Aristotle University of Thessaloniki, 541 24 Thessaloniki, Greece
e-mail: hrisafis@physics.auth.gr

P. Psyllaki
Department of Mechanical Engineering, Technological Education Institute of Piraeus (TEI), 122 44 Egaleo, Greece

Table 1 Typical analysis of the examined steel

Element	C	Si	Mn	Cr	Mo	Al	Fe
wt%	0.03	0.3	6.3	12.0	1.4	1.6	Balance

The manufacturer has accomplished the chemical analysis by mass spectrometry

well polished up to 5 μm alumina emulsion. Their oxidation was studied in a TG-DTA Setaram Setsys 16/18 equipment. The experiments took place in an O_2 atmosphere with a 50 mL/min gas flow, in alumina crucibles and heating rate 1 °C/min, from ambient temperature up to 1000 °C. Isothermal measurements were done for five different temperatures, 725, 775, 800, 825, and 850 °C in O_2 atmosphere for about 12 h. The heating rate from ambient temperature up to the final temperature of the isothermal measurements was 1 °C/min. The online monitoring of the oxidation phenomena with TG allowed the quantitative estimation of oxidation with the continuous recording of mass, temperature, and time. As a result, reliable measurements over a long period of time were recorded, and therefore, a rather precise determination of oxidation kinetics was achieved.

The morphology and the chemical composition of the oxidation products was studied with scanning electron microscopy (SEM) using a 20kVolt JEOL 840A SEM equipped with an OXFORD ISIS 300 EDS analyzer and the necessary software to perform point microanalysis, linear microanalysis, and chemical mapping of the surface under examination. For the SEM examination, the surface of the samples did not undergo any preparation and the examination was direct, while for the examination of the cross section, segments have been cut from each sample, mounted in bakelite and polished down to 5 μm alumina emulsion.

Results and discussion

Initial considerations

For the determination of the isothermal temperatures used for this study, as already mentioned, the material under examination was initially heated with a rate of 1 °C/min up to 1000 °C in oxygen (Fig. 1). From this procedure it was deduced that oxidation till 700 °C is negligible, as the mass change shows. After this temperature the oxidation rate is very low. At about 775 °C the rate increases faster, while after 870 °C the slope of the plot becomes much steeper.

From these observations it could be concluded that the study of the initial stages of oxidation should focus mainly on temperatures above 700 °C. The slope changes of the

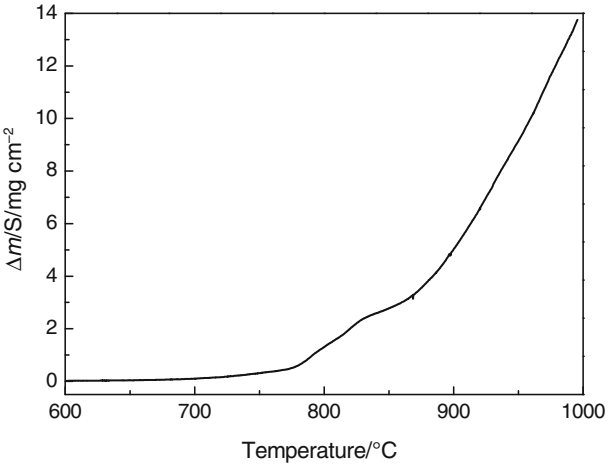

Fig. 1 Mass gain per surface unit vs. temperature in O_2 atmosphere with heating rate 1 °C/min

plot of Fig. 1 indicates that there are at least three different oxidation stages. The first stage expands from ambient temperature up to about 775 °C, the second one from 775 to 830 °C, and the third one covers the area above 830 °C. For this reason it was finally decided to study oxidation at 725, 775, 800, 825, and 850 °C. The final stage of oxidation (mainly above 900 °C) was not examined, as it was discussed in detail elsewhere [8].

SEM–EDS study

Regarding the SEM examination, initially the cross section of the isothermal oxidized samples was observed. Some characteristic micrographs are presented in Fig. 2 showing that the scale thickness increases as the temperature increases and the morphology of the scale changes. At the samples after 12 h oxidation in isothermal temperature of 725 °C two layers compose the scale, which could be distinguished with a difficulty. The thin one at the base metal–scale interface contains a high amount of chromium (along with oxygen), as the EDS analysis shows, while the thick one is mainly composed of iron and oxygen. According to SEM images small pores of different shapes could be observed inside the mass of the thick oxide scale. Similar SEM images have been recorded for the oxidized sample at the isothermal temperature of 775 °C. At the oxidized samples in the isothermal temperature of 800 °C the scale becomes more uniform and the thin layer close to the base metal is not visible any more. However, the number of the pores increases along with their volume. In some cases larger voids are also observed, especially at 825 °C.

However, at the samples oxidized at 850 °C the appearance of the coating becomes more complex, as four layers are now observed. Close to the steel a rather compact zone with considerable thickness is formed. On top of

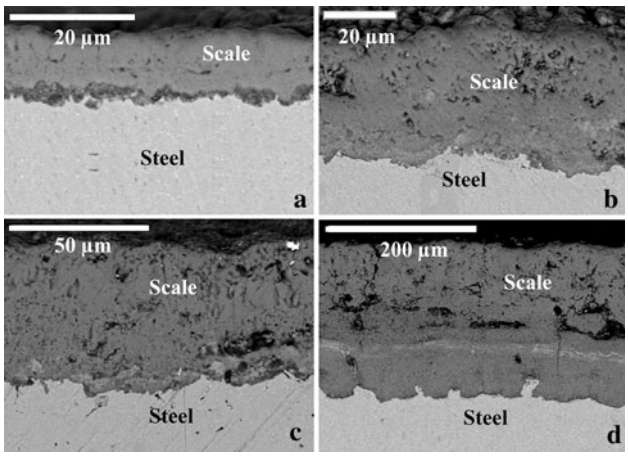

Fig. 2 SEM micrographs (backscattered electrons) of the cross section of the oxidized steel after 12 h of exposure in O_2 atmosphere at **a** 725 °C, **b** 800 °C, **c** 825 °C, and **d** 850 °C

it a thin layer with lighter color is distinguished, while a zone with large voids is present afterward. Finally, the scale is sealed by a layer with smaller pores and cracks.

In this case the EDS analysis of the scale is very useful (Fig. 3). It shows that apart from the different appearance, the layers are also characterized by different composition. Chromium is gathered at the compact zone close to the substrate. In this zone also iron depletion is observed. The thin light-colored layer is characterized by high molybdenum content comparing with the Mo content of the other layers. The next two layers have actually the same composition with each other, although they are characterized by different pore size and different thickness. In the area of these two layers iron is the predominant element. However, at the outer layer increased manganese concentration was also detected. Similar distribution is observed at 800 and

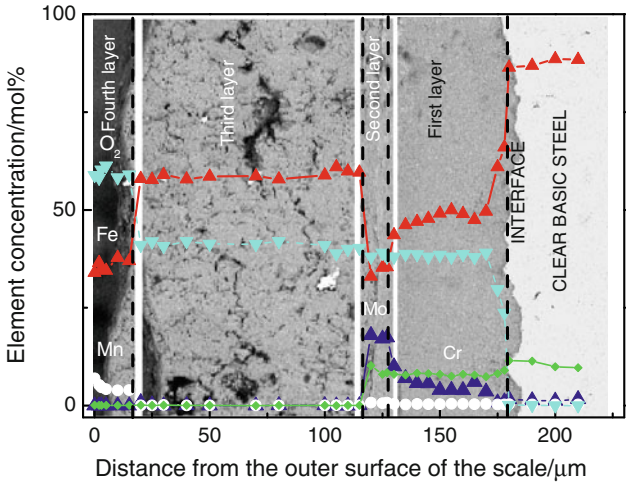

Fig. 3 EDS analysis of the cross section of the oxidized steel after 12 h of exposure in O_2 atmosphere at 850 °C along with an SEM micrograph (backscattered electrons) of the same area

825 °C, while at 725 and 775 °C there is a substantially different morphology at least for the exposure time under examination.

This inhomogeneity is not peculiar. In general, diversification of the oxidation products along the cross section of the scale could be explained with the elementary oxidation theory. A suitable analysis has been presented elsewhere [7]. In the same work the distribution of the pore size is explained. Nevertheless, what is rather impressive is the fact that the scale diversification is likely to be affected by the temperature. It begins only after 800 °C. Below this temperature, only Fe and Cr oxides seem to be present [7].

These observations could be connected to the different oxidation stages of Fig. 1. From the SEM micrographs it seems that during the first oxidation stage, up to about 775 °C, the two-layered scale is present. Between 775 and about 830 °C, the four-layered scale is formed, while after 870 °C the increase of the slope could be related to the increase in the pore number and volume that facilitate the oxygen diffusion through the scale. By contrast up to 775 °C the low rate is likely to be affected by the presence of the inner Cr-rich layer. Probably at such a low temperature this layer impedes the diffusion of Fe ions and as a result oxidation is delayed.

The SEM observation of the plane view of the oxidized specimens could offer some more information (Fig. 4). On the surface of the scale formed at 725 °C two areas could be distinguished. Angular crystals cover part of the substrate while flower-like formations are also observed. The flower-like forms seem to grow on top of the angular crystals. The chemical mapping is also very useful in this case, because it proves that the angular crystals are Cr-rich. By contrast the flower-like formations are Cr-depleted and Fe-rich. It is

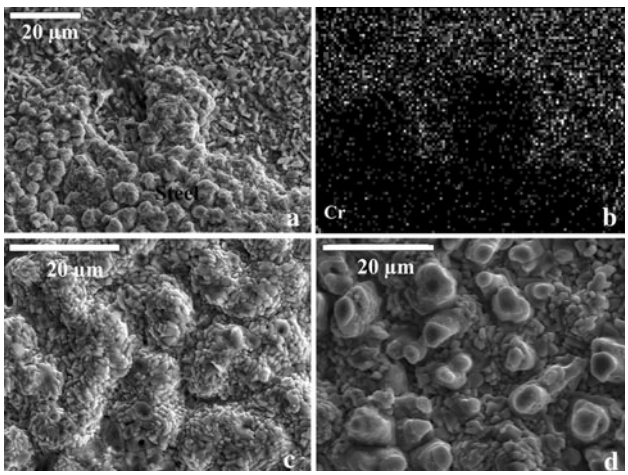

Fig. 4 SEM micrographs (secondary electrons) of the plane view of oxidized steel after 12 h of exposure in O_2 atmosphere at **a** 725, **c** 800, and **d** 850 °C, along with the chemical mapping of the surface exposed at 725 °C (**b**), where the areas with high Cr content are light-colored

obvious that these phases refer to the layers previously observed at this temperature. The angular crystals form the Cr-rich layer and the flower-like formations refer to Fe oxides. Hence the Cr layer is formed first. Actually at the surface of ferritic stainless steels, containing more than 17% Cr, a layer of Cr_2O_3 (thermal oxide, with an average thickness of a few nm) is always present. This layer ensures the corrosion and oxidation resistance of these alloys. Thus it seems that initially this layer grows and afterward the layer of the Fe oxides grows with Fe diffusion through the Cr layer. Finally the Fe oxides cover surface of the substrate. Their formations continue to grow as temperature increases and a surface with a peculiar relief is created, which looks like a living tissue.

Kinetics

The most efficient way to estimate the performance of a material in an oxidizing environment at constant temperature is to consider its mass change with regard to the exposure time. As a matter of fact, in the case of a ferrous material, the reaction of oxygen with iron results to a mass gain Δm of the exposed specimen. The mass gain is a function of the exposure time t in the aggressive environment, while the rest of the factors affecting the phenomenon are incorporated in a constant k_p. Hence, the comparison of the performance is reduced to the determination of the function that binds Δm and t along with the calculation of the constant k_p.

For the oxidation of a metallic material, it is usually considered that kinetics obey a parabolic law [1–5]. Hence, the mass gain per unit area can be expressed as the following:

$$\Delta m^2 = k_p t$$

where Δm is the mass gain per unit area at time t and k_p is the rate constant. However, according to Pieraggi and other works [9–11] the plot of the kinetics data as Δm vs. $t^{1/2}$ is inherently superior to the Δm^2 vs. t plot for the determination of a parabolic rate constant following some faster transient growth of an initial scale.

In the case under study, the results of the isothermal study are summarized in the plots of Fig. 5, which offer important information. First of all, as it was deduced from the SEM micrographs, oxidation is more intense as isothermal temperature increases. Furthermore, there is a characteristic similarity between the different curves. Oxidation is impeded with regard to the exposure time. This means that the scale formed is rather protective, and its growth decreases the rate of the phenomenon.

Nevertheless, the oxidation progress at every temperature does not follow the same pattern. At 775 °C a continuous, smooth line is observed, while the mass gain for the temperature of 725 °C the mass gain was very small

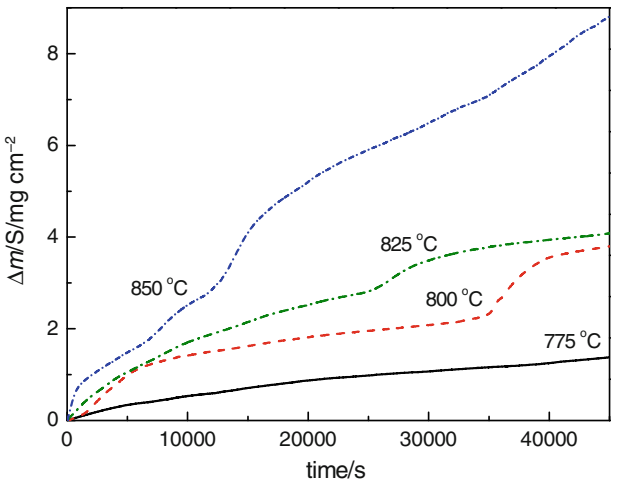

Fig. 5 Evolution of the mass gain per unit area (Δm/S) as a function of the oxidation time (t) for four different isothermal temperatures

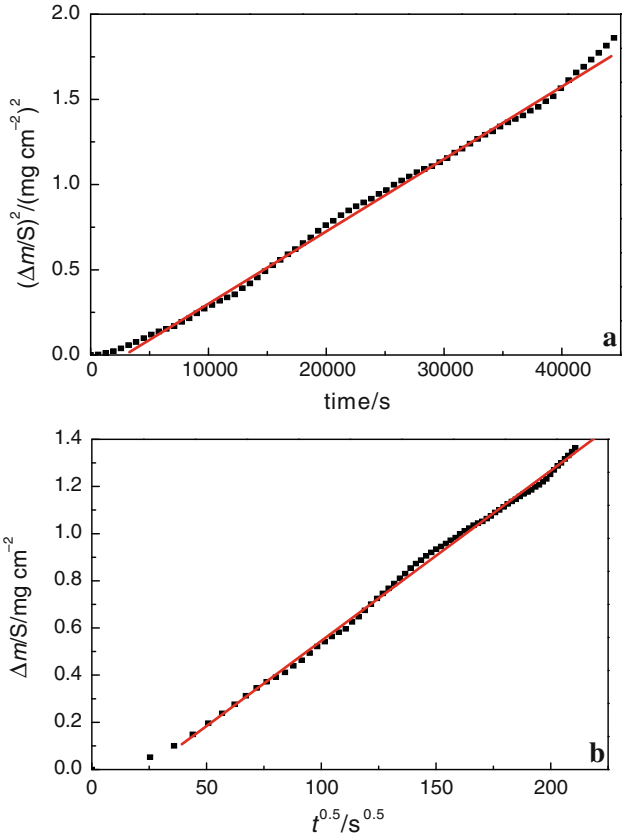

Fig. 6 Mass gain per unit area $(\Delta m/S)^2$ as a function of time (**a**) and mass gain per unit area (Δm/S) as a function of square root of time (**b**) during oxidation at 775 °C

and for this reason these data were not used for the kinetics calculation. By contrast at 800, 825, and 850 °C, although the curves are continuous, they are not smooth. After certain exposure periods, which are different for every line,

their slope is changed. Obviously this phenomenon, which causes an intense variation of the oxidation rate, is related to the changes in the scale structure that were previously mentioned and undoubtedly affect the oxidation mechanism

These conclusions could be further clarified if the same data are presented using the correlations Δm^2 vs. t and Δm vs. $t^{1/2}$. Figure 6a summarizes the results at 775 °C, when the parabolic function Δm^2 vs. t is used. The result is not unexpected. This plot indicates that at this temperature a straight line could describe oxidation progress with reasonable accuracy. Hence the initial assumption is true. The deviation from this behavior, which is observed for low heating time, could be explained by assuming that, initially, transient oxidation phenomena take place, which after a certain exposure period, result to the formation of a stable scale. Diffusion through this scale is the controlling step and hence the mass change rate becomes parabolic. The same conclusions are also drawn when the plot of Δm vs. $t^{1/2}$ is used (Fig. 6b). The same analysis was accomplished for the data of the experiments performed at the other temperatures. In Fig. 7a and b the plots at 825 °C are presented, while the similar plots could be connected with

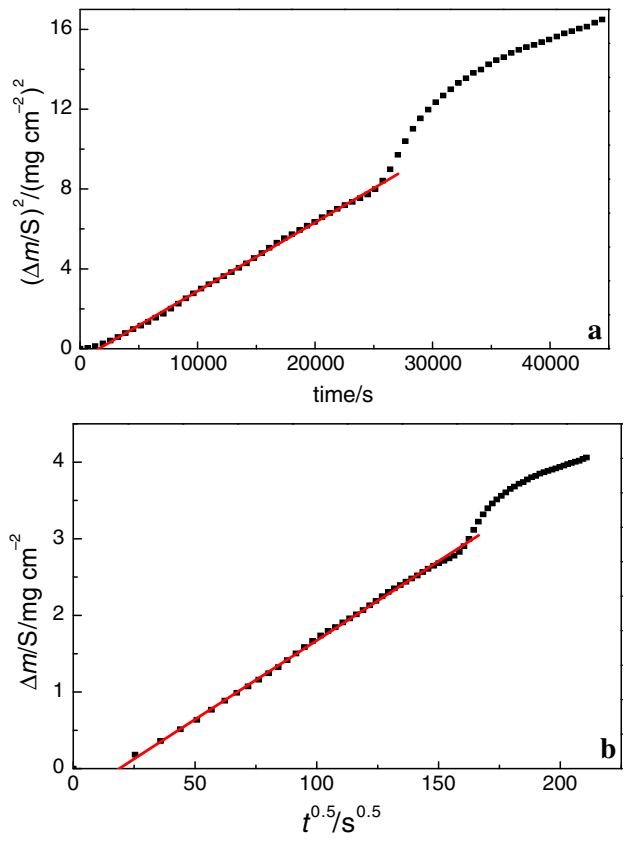

Fig. 7 Mass gain per unit area $(\Delta m/S)^2$ as a function of time (**a**) and mass gain per unit area $(\Delta m/S)$ as a function of square root of time during oxidation (**b**) obtained at 825 °C

Table 2 Calculated values of the rate constant k_p at three isothermal temperatures

T/°C	k_p from Δm^2 vs. t	k_p from Δm vs. $t^{1/2}$
775	4.25×10^{-5}	5.21×10^{-5}
800	1.16×10^{-4}	8.39×10^{-5}
825	3.44×10^{-4}	4.24×10^{-4}
850	1.51×10^{-3}	1.63×10^{-3}

The regression factors are greater than 0.999

the results of oxidation at 800 and 850 °C. The difference with the results at 775 °C is obvious. The straight line is followed by a curve after a certain incubation period. The necessary exposure time for the appearance of the curve decreases as temperature increases. Furthermore its slope is lower. Hence after a certain exposure time a change in the scale structure takes place which decreases oxidation rate.

From the plots of Figs. 6 and 7 the values of the rate constant k_p were calculated. These results are summarized in Table 2 and refer only to the linear part of each curve. In any case the results are very similar regardless the law used. This means that the behavior of the function is very close to parabolic. Furthermore, as it was expected, the values are almost two orders of magnitude lower than the results for the "steady-state" oxidation [8]. Hence the rate constant increases as the oxidation temperature increases. Obviously, oxidation is more intense at higher temperature.

Furthermore, the Arrhenius law could be used for the same data:

$$k_p = k_o \exp(-E/RT)$$

where k_o is the pre-exponential factor, E is the apparent activation energy, R is the gas constant, and T is the absolute temperature. The curve of the logarithm of k_p versus $1000/T$ for the values of k_p from this equation is

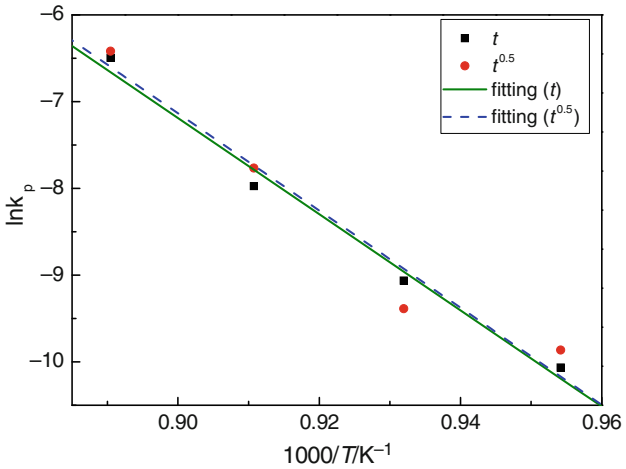

Fig. 8 Dependence of the parabolic rate constant of oxidation of the temperature

Table 3 Calculated values of the activation energy

Equation	Activation energy E/kJ mol^{-1}	Regression factor
Δm^2 vs. t	460.8	0.994
Δm vs. $t^{1/2}$	466.0	0.977

shown in Fig. 8. From this diagram E could be calculated. The results are summarized in Table 3. The determined values are very similar to each other, as the initial data (k_p) were very close to each other. This result shows that the two methods used for the calculation of k_p could be applied quite well to the examined experiments. However, the activation energy is almost four times the activation energy for "steady-state" [8]. Hence, the oxidation phenomena that take place during the transitional period provide another barrier to the deterioration of the ferrous base metal and as a result they offer increased protection.

Conclusions

The oxidation of PH steel is accomplished at three steps at the minimum. Up to 775 °C a two-layered scale is formed, while above this temperature the scale is composed of four layers. After 850 °C no more morphological changes are observed. The four-layered structure remains and oxidation rate increases due to the increase in the pore number and volume that facilitate the oxygen diffusion through the scale. As far as the kinetic curves are concerned, by which the rate constant k_p and the activation energy were calculated, a transitional and a steady-state period are also observed. The comparison of the data of these two periods shows that the oxidation rate during the transitional period is much lower. Hence the oxidation phenomena during this phase provide another barrier to the deterioration of the ferrous material and as a result they offer increased protection.

References

1. Davis JR. Heat-resistant materials. 3rd ed. New York: ASM International; 1997.
2. Wright I. High temperature corrosion. In: Davis LO, editor. ASM handbook, vol. 13. New York: ASM International; 1997. p. 97–101.
3. Kofstad P. High temperature corrosion. 3rd ed. New York: Elsevier Applied Science; 1988.
4. Fontana MG. Corrosion engineering. 3rd ed. New York: McGraw-Hill; 1986.
5. Birks N, Meier GH. Introduction to high temperature oxidation of metals. 2nd ed. London: Edward Arnold; 1983.
6. Washko SD, Aggen G. Wrought stainless steels. In: Davis LO, editor. ASM handbook, vol. 1. New York: ASM International; 1997. p. 1303–408.
7. Vourlias G, Pistofidis N, Pavlidou E, Chrissafis K. Oxidation behaviour of precipitation hardened steel TG, X-ray, XRD and SEM study. J Therm Anal Calorim. 2009;95:63–8.
8. Vourlias G, Pistofidis N, Chrissafis K. High-temperature oxidation of precipitation hardening steel. Thermochim Acta. 2008;478: 28–33.
9. Pieraggi B. Calculations of parabolic reaction rate constants. Oxid Met. 1987;27:177–85.
10. Levy M, Farrell P, Pettit F. Oxidation of some advanced single-crystal nickel-base superalloys in air at 2000°F (1093°C). Corrosion. 1986;42:708–17.
11. Pieraggi B, Rapp RA. Chromia scale growth in alloy oxidation and the reactive element effect. J Electrochem Soc. 1993;140: 2844–50.